JOURNAL OF THERMOPHYSICS AND HEAT TRANSFER
Vol. 9, No. 2, April–June 1995

Natural Convection in Inclined Enclosures with Multiple Conducting Partitions

A. Kangni,* P. Vasseur,† and E. Bilgen‡
University of Montreal, Montreal, Quebec H3C 3A7, Canada

Laminar natural convection and conduction in inclined enclosures having multiple partitions with finite thickness and conductivity have been studied theoretically. The governing equations are solved using finite difference formulation and a volume control method. The study covers the range of Ra from 10^3 to 10^7, Φ from 0 to 180 deg, $A = H/W$ from 1 to 20, $B = w/W$ from 0.1 to 0.9, $C = l/W$ from 0.01 to 0.1, and the thermal conductivity ratio of partition to fluid k_r from 1 to 10^4. The partition number N was varied from 1 to 5. The Prandtl number was 0.72 (for air). The results are reduced in terms of Nu as a function of Ra, k_r, Φ, and various geometrical parameters (A, B, C). The streamlines and isotherms are produced to visualize the flow and temperature fields.

Nomenclature

A = enclosure aspect ratio, H/W
B = dimensionless cavity width, w/W
C = dimensionless partition thickness, l/W
g = acceleration due to gravity, m/s^2
H = height of enclosure, m
k = thermal conductivity, W/m$^2\cdot$K
L = general thermal diffusion coefficient
l = partition thickness, m
N = number of partitions
Nu = Nusselt number, hW/k
Nu_{loc} = local Nusselt number, hx/k
P = dimensionless pressure, $[p + \rho g(y \sin \Phi - x \cos \Phi)]/[\rho(\alpha/W)^2]$
Pr = Prandtl number, ν/α
p = pressure, Pa
Ra = Rayleigh number, $g\beta\Delta TW^3/(\nu\alpha)$
T = temperature, K
U, V = dimensionless fluid velocities, uW/α, vW/α
W = width of enclosure, m
w = width of cavity, m
X, Y = dimensionless distance on x and y, x/W, y/W
α = thermal diffusivity, $k/(\rho c_p)$, m^2/s
β = thermal expansion of fluid, 1/K
Γ = general viscous diffusion coefficient
ΔT = temperature difference, $T_2 - T_1$
$\delta x, \delta y$ = grid size
η = thermal efficiency
θ = dimensionless temperature, $(T - T_1)/\Delta T$
ν = kinematic viscosity, m^2/s
ρ = fluid density, kg/m^3
Φ = inclination angle of the hot plate from the horizontal plane, deg

Subscripts

f = fluid
r = ratio partition to fluid
w = partition wall
1 = cold wall, left bounding wall
2 = hot wall, right bounding wall

Received April 20, 1994; revision received Oct. 20, 1994; accepted for publication Oct. 21, 1994.

*Graduate Research Assistant, Mechanical Engineering Department, École Polytechnique.
†Professor, Mechanical Engineering Department, École Polytechnique.
‡Professor, Mechanical Engineering Department, École Polytechnique.

Introduction

IN many practical cases, enclosures with vertical partitions are used to modify heat transfer by natural convection, conduction, or radiation. The interest in such problems stems from their importance in such areas as the design of building components for energy conservation, thermal design of double pane windows, and solar collector applications. The problem of primary interest in the literature is that of an enclosure with no partitions, excellent reviews have been presented in the literature.[1] Despite their importance, little attention has been given to investigations of heat transfer within enclosures containing partitions. A literature review shows that there have been various theoretical and experimental studies on natural convection in enclosures with single and multiple diathermal partitions:

1) Studies with a single partition were in vertical enclosures[2,3] and in inclined enclosures.[4]

2) Studies with multiple partitions in vertical enclosures included double partition[5] and multiple partitions.[6,7] The boundary conditions in these studies consisted of two isothermal vertical bounding walls and two adiabatic horizontal bounding walls with equally spaced partitions. The effect of an off-center partition on natural convection heat transfer has also been reported by Nishimura et al.[8] The effects of conductivity of equally spaced and off-center partitions have been reported by Kangni et al.[9] The results of earlier studies show that the heat transfer rates through the system with partitions decrease with increasing number of partition.

Anderson and Bejan[5] studied the enclosures with a single partition analytically based on the Oseen linearization method. The study was in the boundary-layer regime and the effect of the conductance through the partition was supposed to be negligible. They confirmed their results experimentally using an enclosure with a double partition. The experimental results were correlated to obtain a relation of heat transfer between the two ends. It was proportional to $(1 + N)^{-0.61}$. Nishimura et al.[7,8] have used a boundary-layer solution and confirmed their results experimentally for the case of an enclosure with an off-center partition as well as with equally distanced multiple partitions. They also extended their study to nonboundary-layer regime by a numerical study. They showed that the isothermal partition model was not suitable for multiple partitions and they derived a correlation for heat transfer between the two ends. It was proportional to $(1 + N)^{-1}$ in

the boundary-layer regime where the boundary-layer thickness is smaller than the half-width of each cell. Acharya and Tsang[4] have studied inclined enclosures with a centrally located partition using a finite difference procedure. Chen et al.[10] studied numerically inclined partitioned enclosures of solar collectors and considered the heat conduction through the partitions. The range of Rayleigh number investigated was up to 5×10^4. Kangni et al.[9] studied numerically the heat transfer by natural convection and conduction in vertical enclosures having vertical partitions with finite thickness and conductivity at a range of the Rayleigh number of 10^3–10^7.

There are several practical cases, such as composite solar collector systems,[11] with several off-center partitions in an inclined enclosure, having finite thickness and finite conductivity and operating in both boundary-layer and nonboundary-layer regimes. The magnitudes of conductivity ratios of practical materials to air are about 10 deg for insulating materials, 10^1–10^2 for glass, various woods, gypsum plates, concrete, and brick; and 10^3–10^4 for metals. The inclination angle may vary from vertical to horizontal. These cases are not considered in the literature and will be addressed in this study.

Problem Description and Mathematical Model

The schematic of the system with the coordinates and boundary conditions are shown in Fig. 1. The aspect ratio $A = H/W$ was varied from 1 to 20. The partitions were off-center and had a variable thickness l. The nondimensional thickness $C = l/W$ was varied from 0.01 to 0.1, and the nondimensional width $B = w/W$ varied from 0.1 to 0.9.

The flow is assumed to be steady, laminar, and two dimensional. The third dimension of the channel (direction perpendicular to the figure) is large enough so that the flow and heat transfer are two dimensional. It is known that this assumption holds true for all cases except near horizontal configurations. Near horizontal configurations of longitudinal enclosures the two-dimensional model with the infinite third dimension is not capable to describe the physical phenomenon. In this case, thermal instabilities result in longitudinal vortices, which make the problem a three-dimensional one.[12,13] Various studies show the three-dimensional aspect of natural convection in rectangular cavities at horizontal and near horizontal positions.[14] In particular, Ozoe et al.[15] provide theoretical and experimental results showing quasi-two-dimensional cells at the horizontal position, three-dimensional oblique cells between horizontal and a critical inclination angle, and two-dimensional cells at higher inclinations.

Partitioned cavities at and near horizontal configurations in this study represent the limiting case, and a literature review shows that there are no studies concerning three-dimensional aspect in cavities with multiple partitions at small inclination angles. This aspect will further be studied and discussed later when the effect of the inclination angle is presented.

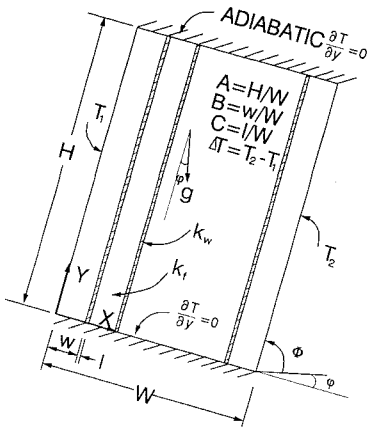

Fig. 1 Schematic of the problem and the coordinate system.

The Boussinesq approximation is used to account for the density variation. The governing equations are nondimensionalized by using the nondimensional parameters defined in the nomenclature. The resulting continuity, momentum, and energy equations are

$$\frac{\partial U}{\partial X} + \frac{\partial V}{\partial Y} = 0 \tag{1}$$

$$U\frac{\partial U}{\partial X} + V\frac{\partial U}{\partial Y} = -\frac{\partial P}{\partial X} + \Gamma Pr\nabla^2 U - PrRa\cos\Phi\,\theta \tag{2}$$

$$U\frac{\partial V}{\partial X} + V\frac{\partial V}{\partial Y} = -\frac{\partial P}{\partial Y} + \Gamma Pr\nabla^2 V + PrRa\sin\Phi\,\theta \tag{3}$$

$$U\frac{\partial \theta}{\partial X} + V\frac{\partial \theta}{\partial Y} = L\nabla^2\theta \tag{4}$$

where Γ is a general diffusion coefficient, which is equal to 1 in the fluid region and ∞ in the solid region, and L is equal to 1 in the fluid region and k_r in the solid region. The coefficients Γ and L are introduced in the discretized equations to ensure that the conduction in the partitions is accounted for and that $U = V = 0$ everywhere in the solid region including at solid–fluid interfaces. Normally, the heat flux from the other surfaces is deduced from the results of the computations.

The boundary conditions are the no-slip conditions on all the rigid wall surfaces, isothermal temperature on the long side walls, and adiabatic on the short end walls (see Fig. 1):

$$0 \le X \le 1, \qquad Y = 0, A \quad \frac{\partial \theta}{\partial Y} = 0 \tag{5}$$

$$0 \le Y \le A, \qquad X = 0 \quad \theta = 0 \tag{6}$$

$$X = 1 \quad \theta = 1 \tag{7}$$

The numerical method used to solve the system of Eqs. (1–4) is the simpler method.[16] This algorithm is based on a control volume approach, and the equations are discretized by ensuring that conservations of mass, momentum, and energy are satisfied over each control volume. To avoid a wavy pressure and velocity fields, a staggered grid for velocity is used as suggested in Ref. 16.

The heat transfer from the left and right bounding walls is calculated as

$$Nu = \frac{\displaystyle\int_0^A \left.\frac{\partial \theta}{\partial X}\right|_{X=0} dY}{\displaystyle\int_0^A \left.\frac{\partial \theta}{\partial X}\right|_{X=0} dY\Bigg|_{\text{cond}}} \tag{8}$$

The stream function is calculated from its definition

$$U = -\frac{\partial \Psi}{\partial Y}, \qquad V = \frac{\partial \Psi}{\partial X} \tag{9}$$

and by assuming $\Psi = 0$ at the boundaries.

Validation of the Code and Computation

The computer code based on the mathematical model above and the simpler method are validated for various cases and the results are published elsewhere.[17] In summary, the deviations from the benchmark solutions[18] for $Ra = 10^6$ were 4.66% in Ψ_{max}, 3.34% in U_{max}, 1.55% in V_{max}, and 6.81% in Nu_0. The comparison was also made with the results of Le Breton et al.,[19] who used the same solution technique as in

this study. The maximum deviations of the same parameters were 2.3, 1.4, 0.7, and 1.1%, respectively. A uniform grid size in Y direction and nonuniform in X direction were used in this study. The uniform grid size in Y direction was varied from 21 for $\phi = 0$ deg to 25 for 90 deg. That in X direction had a minimum of three control volumes in each partition (solid media) and a minimum of four control volumes between the partitions (fluid media). For example, with 2 partitions there were 3 control volumes in each partition, 9 in fluid media and 1 at each side of the cavity, making 35 control volumes in X direction. The independence of solution on the grid size was studied for various cases and k_r. For instance, with two partitions and for various Rayleigh numbers, the grid sizes of 14×14, 21×21, and 26×26 (all with three control volumes in each partition), and 30×30, 33×33, 36×36, 39×39, 42×42, and 45×45 (all with five control volumes in each partition) were used. The results showed that grid independence was achieved above 25, showing negligible differences in heat transfer and Ψ_{max}. In any case, the Nusselt numbers for various k_r showed similar trends as a function of grid size, ensuring the observed conclusion of grid independence.

For small Rayleigh numbers, the number of iterations was about 35. For larger Ra, the solution from the smaller Ra was used to initialize the computation so that the number of iterations was reduced considerably. The relaxation parameter was varied from 0.80–0.70 for small Ra to about 0.40 for large Ra. The execution time for a typical case with $Ra = 10^5$ and 20 iterations was 12 CPU time on IBM 3090 with 17 mips.

The convergence criteria was based on the corrected pressure field. When the corrected terms were small enough so that no difference existed between the pressure field before and after correction, the computation was stopped. Therefore,

$$\sum b_{ij} < \varepsilon \tag{10}$$

where ε was from 10^{-3} to 10^{-4}. In addition to the usual accuracy control, the accuracy of computations was controlled using the energy conservation within the system.

Results and Discussion

Various computations were carried out for the ranges of geometrical parameters discussed earlier and the Rayleigh number from 10^3 to 10^7. The fluid was air with $Pr = 0.72$. The aspect ratio A was varied from 1 to 20. The results are represented to carry out parametric studies on the influence of various dimensionless parameters, namely A, B, C, Φ, N, and k_r. First, the results with $A = 1$ will be presented and then its effect will be discussed.

General Observations

The stream functions and isotherms for the case of $A = 1$, $C = 0.01$, $k_r = 10$, various Φ, and for $Ra = 10^6$ are presented in Fig. 2. The results with the partition number of 1, 5, and for $\Phi = 90$ deg, i.e., for vertical position, are shown in Figs. 2a and 2b. Similar results for $\Phi = 60$ deg are shown in Figs. 2c and 2d. With partition numbers of 1, 3, and for $\Phi = 0$ deg, i.e., for horizontal position, they are shown in Figs. 2e and 2f. The isotherms in Figs. 2a and 2b for the vertical case show that the convection with stratification is dominant with one partition, and a boundary-layer regime is present. It is less dominant with increasing partition numbers, and the conduction regime becomes a dominant heat transfer mode for five partitions. For the case under consideration the partitions are relatively thin and their diffusivity is 10 times higher than that of air. Therefore, very little effect due to partitions is observable. The streamlines on the left side of each figure and their intensity given in the figure show that the convection intensity is identical at both sides of the bounding left and right walls. It decreases in the middle cavities with more than one partition. The intensity decreases with increasing partition numbers, confirming the observation made with isotherms. Similar observations can be made in Figs. 2c and 2d for the inclined case. With one partition, Fig. 2c shows more intense circulation and increased convection with respect to Fig. 2a. Similar observations are made in Figs. 2b and 2d. The heat transfer is obviously increased for an inclined cavity. Figures 2e and 2f show the isotherms and streamlines for the limiting case of horizontal position. Two counter-rotating cells are formed with one partition, and four with three. The isotherms show that the fluid rises in the middle and the circulation is natural (see, e.g., Hasnaoui et al.[20] for the case without partitions and natural–antinatural circulations). In Fig. 2e, near the bottom, at the partition and the top, the heat transfer is by conduction. The case with three partitions in Fig. 2f is similar, however, with less convection. The fluid rises at two locations, resulting in a downward flow at the center of each horizontal cavity. The streamlines on the left of these figures show that the convection intensity is decreased with increasing number of partitions. They are, however, increased with respect to the other corresponding cases of Fig. 2. The intensities are lower at the upper cavity in Fig. 2e and in the middle cavities in Fig. 2f.

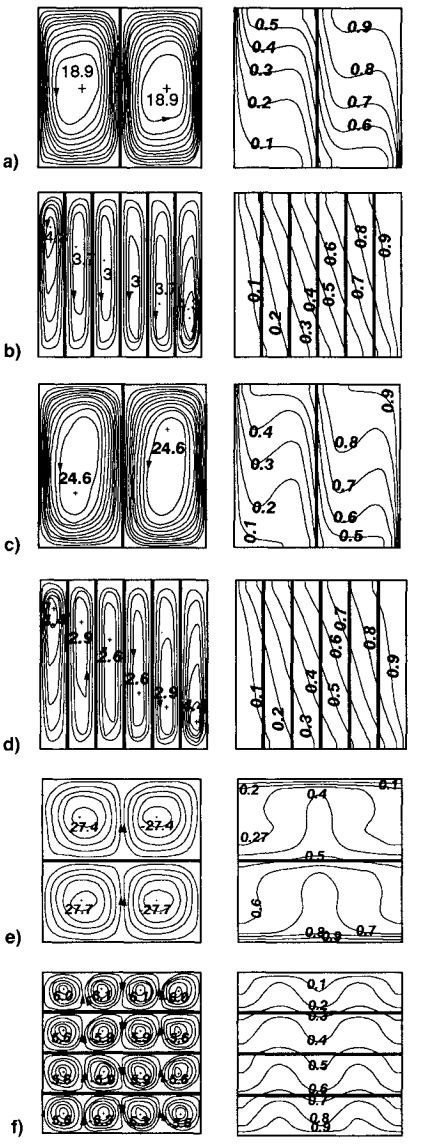

Fig. 2 Streamlines (on the left) and isotherms (on the right) for $Ra = 10^6$, $C = 0.01$, $k_r = 10$. Φ = a), b) 90; c), d) 60; and e), f) 0 deg.

Streamlines and isotherms for the case of Fig. 2c, but with $Ra = 10^5$ and 10^3, showed (not presented in a figure) that,

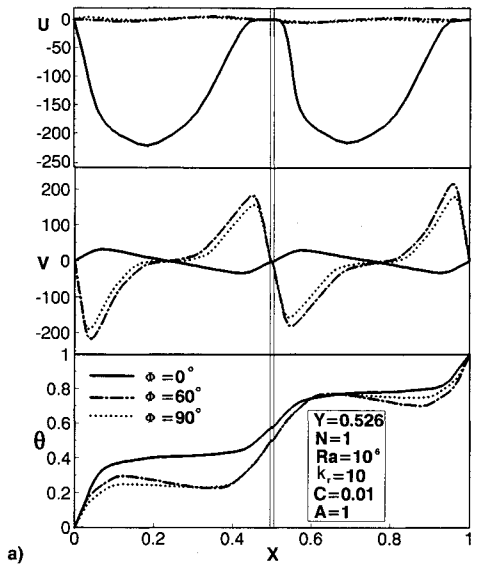

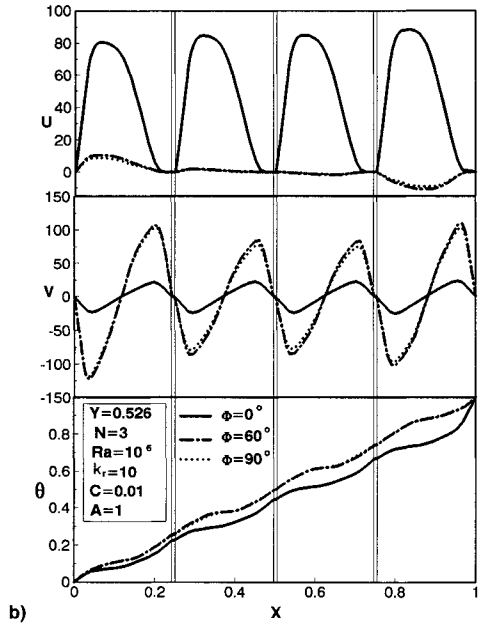

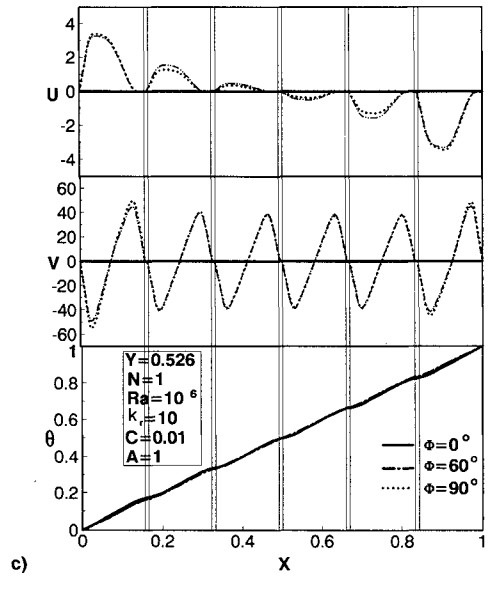

Fig. 3 Velocity profiles in x and y directions and temperature profile at the midheight. N = a) 1, b) 3, and c) 5.

as expected, the effect of convection was reduced with decreasing Ra. The dominant heat transfer mode was by conduction at $Ra = 10^3$. The streamlines and their intensities showed that the convection intensities were decreased with decreasing Ra, confirming the earlier observations.

The velocity profiles and dimensionless temperature at $Y = 0.526$ (almost at midheight), for $Ra = 10^6$, $k_r = 10$, $C = 0.01$, $\Phi = 90$, 60, and 0 deg, are presented in Figs. 3a–3c for $N = 1, 3, 5$, respectively. Figure 3a shows the results with one partition. For $\Phi = 90$ and 60 deg, the X velocity component is very small and the Y velocity component shows an anticlockwise circulation in the two cavities. For $\Phi = 0$ deg, the X velocity component shows the rising fluid in the center. The Y velocity component is moderate in this case. The temperature profiles show that the temperature in the cavities becomes more uniform as the inclination angle decreases. With increasing partition number, similar observations can be made. However, it is seen that the magnitudes of the velocity components become smaller with increasing N, showing less convection. It should also be noticed that the convection is stronger at the right and left bounding walls. The

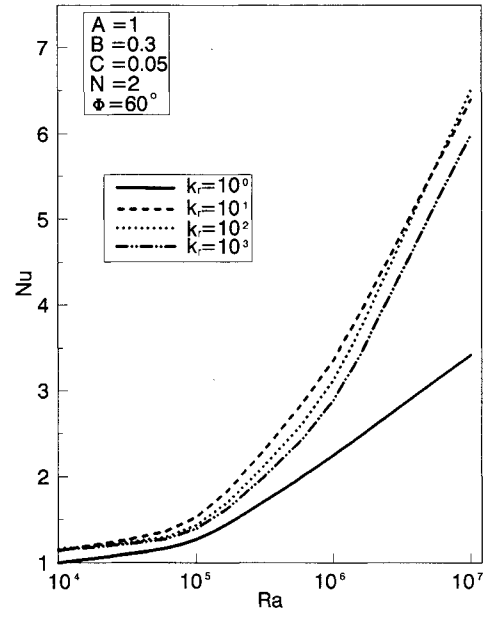

Fig. 4 Nu as a function of Ra with k_r parametric variable.

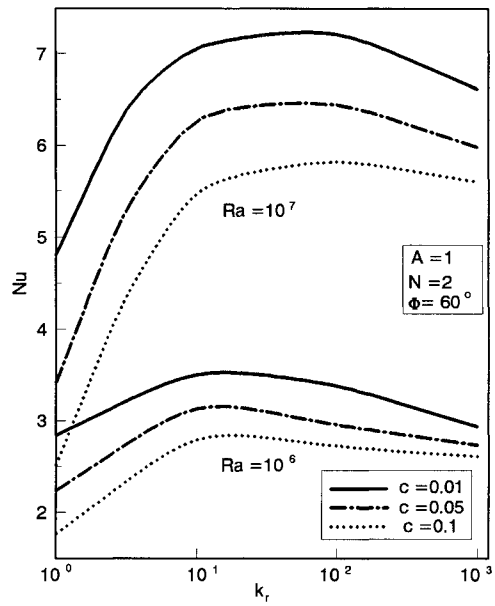

Fig. 5 Nu as a function of k_r with C and Ra parametric variables.

temperature profiles become linear with increasing N. These quantitative results support the general observations made earlier.

Effect of k_r for Various C

Nu as a function of Ra is presented for the case of $A = 1$, $B = 0.3$, $C = 0.05$, $N = 2$, $\Phi = 60$ deg, and for various k_r in Fig. 4. The effect of k_r on Nu for various C and Ra is presented in Fig. 5. Figure 4 shows that Nu is generally an increasing function of k_r. However, as Ra increases, it becomes a decreasing function of k_r when it is higher than a characteristic value. Figure 5 presents the results with $Ra = 10^6$ and 10^7 that clearly show Nu passing from a maximum at a k_r for each case. It is seen that Nu is a decreasing function of C. This is because the fluid layer occupies more space with decreasing partition thickness, and the heat transfer by convection increases at high Ra. It was observed (not shown here) that Nu was an increasing function of C at low Ra, showing that the dominant heat transfer is by conduction.

To explain the maximum Nu at a characteristic k_r, the streamlines and isotherms were examined. The results for $Ra = 10^7$, $C = 0.01$, and for various k_r are shown in Fig. 6a–6c. It is noticed that the convection intensity increases with increasing k_r in each enclosure. For instance, Ψ_{max} varies from 41.5 for $k_r = 10$ to 48.3 for $k_r = 10^3$ in the left and right enclosure. Although Ψ_{max} is an increasing function of k_r, its gradient, defining the velocity components according to Eq. (9), varies first as an increasing function of k_r, and then as a decreasing function of it. Since the energy transport from the hot to cold wall follows the heat lines, the transverse velocity component $U \sim \Delta\Psi/\Delta Y$ should be considered in deducing the effect of the gradient of Ψ on Nu.[21] In fact, $(\Psi_{max} - \Psi_{Y=0})/\Delta Y = \Psi_{max}/\Delta Y$ at the right enclosure of Fig. 6, for instance, are calculated as 77.1 for $k_r = 10$, 117.5 for $k_r = 10^2$, 77.5 for $k_r = 10^3$. From the scale analysis, it is known that $u \sim (\alpha/H)Ra_H^{1/2}$, $Nu \sim Ra_H^{1/4}$; therefore, $Nu \sim u^{1/2}$.[22] $\Psi_{max}/\Delta Y$ being proportional to the average flow rate or the average velocity, $Nu \sim$ (gradient of Ψ)$^{1/2}$. As a result, it is expected that Nu first increases then decreases with increasing k_r, as observed in Fig. 5. It is also seen that the temperature gradient across the cavities in Fig. 6 increases up to a characteristic value of $k_r \approx 100$, and then decreases, particularly near the left and right boundaries. The variations of isotherms 0.1 and 0.3 on the left side and for $k_r = 10$, 100, and 10^3, clearly show that the temperature gradient for $k_r = 100$ is the highest.

Variations of local Nusselt numbers along the left, right bounding walls, and on the partitions were studied for the same case as of Fig. 6. The results at the left and right bounding walls ($X = 0$ and 1) are presented in Fig. 7. It is seen that the local Nusselt number increases with increasing k_r up to 100 and then decreases. This is particularly so near the bottom on the left and near the top on the right side bounding walls. The local Nusselt numbers along the partitions (not shown here) varied as an increasing function of k_r, supporting the observations and explanation above.

Effect of B

The effect of B on heat transfer with C and k_r, taken as parameters, is shown in Fig. 8 for the case of $A = 1$, $N = 1$, $\Phi = 60$ deg, and $Ra = 10^6$. For a given C and k_r, Fig. 8 shows that Nu increases with decreasing B, i.e., the off-center partitions are less effective to decrease the heat transfer. At high B, the heat transfer increases with increasing k_r up to a critical k_r, and then decreases slightly. This phenomenon was observed and discussed with Figs. 4 and 5. It is seen that at low B, Nu is an increasing function of k_r. To explain this, the streamlines and isotherms were produced (not shown). It was seen that the heat transfer in the smaller cavity was dominated by conduction and the increased heat transfer was due to more violent convection in the larger cavity. The higher conductivity of the partition was a factor in enhancing the heat transfer.

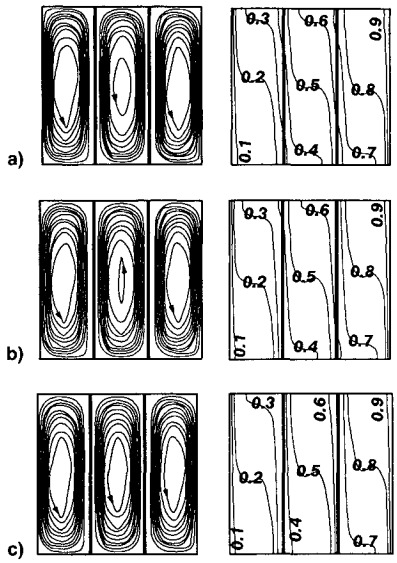

Fig. 6 Streamlines (on the left) and isotherms (on the right) for the same condition as in Fig. 5 and $Ra = 10^7$: a) $k_r = 10$, $\Psi_{max} = 41.5$ at ($X = 0.15$, $Y = 0.54$), $\Psi_{max} = 36.3$ at ($X = 0$, $Y = 0.46$), $\Psi_{max} = 41.5$ at ($X = 0.85$, $Y = 0.54$); b) $k_r = 10^2$, $\Psi_{max} = 45.2$ at ($X = 0.15$, $Y = 0.38$), $\Psi_{max} = 42.0$ at ($X = 0.5$, $Y = 0.54$), $\Psi_{max} = 45.2$ at ($X = 0.85$, $Y = 0.62$); c) $k_r = 10^3$, $\Psi_{max} = 48.3$ at ($X = 0.15$, $Y = 0.31$), $\Psi_{max} = 47.4$ at ($X = 0.5$, $Y = 0.38$), $\Psi_{max} = 48.3$ at ($X = 0.85$, $Y = 0.38$).

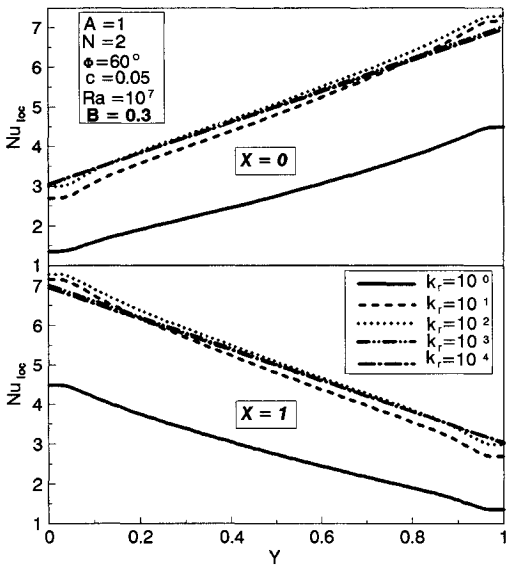

Fig. 7 Local Nu number along the bounding walls for various k_r and $Ra = 10^7$. Other parameters are shown in the figure.

Therefore, Nu increased with increasing k_r. Figure 8 shows also that Nu decreases with increasing C, since the convection decreases in resulting smaller cavities.

Effect of Φ

Before studying the effect of Φ on Nu in partitioned cavities, the case of a cavity without partition near horizontal configuration was studied. The geometrical and dynamical conditions of square cavity studied by Ozoe et al.[15] and their Fig. 3 were taken as base: $A = 1$, $Pr = 10$, $Ra = 4 \times 10^4$, with $\delta x = \delta y = 0.125$. It was seen that the two-dimensional model produced results within +5.5% (in average) in the range of Φ from 0 to 30 deg. The deviation became less as Φ increased. It was then concluded that the two-dimensional model near horizontal configurations of partitioned cavities would produce results with correct order of magnitude, but they should be treated with caution. The results near hori-

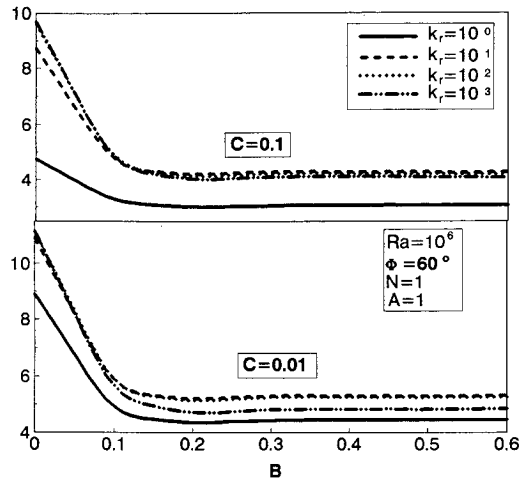

Fig. 8 *Nu* as function of *B* with *Ra*, *C*, and k_r as parametric variables.

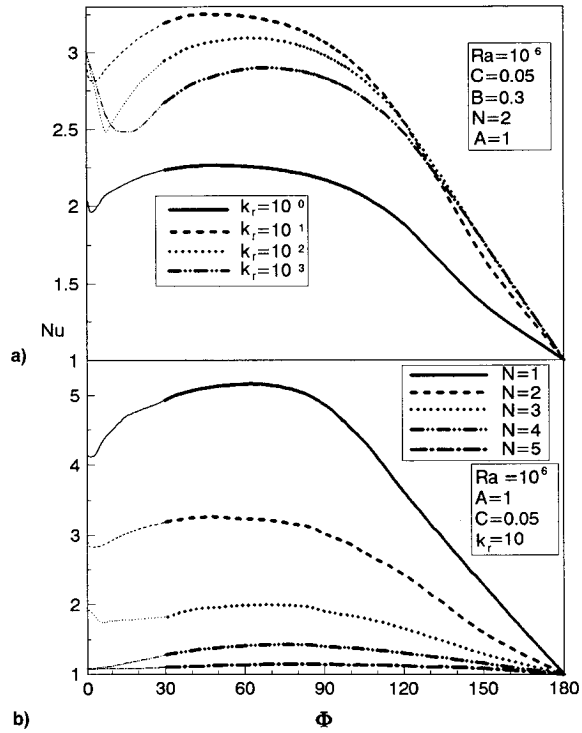

Fig. 9 *Nu* as a function of Φ: a) k_r as variable and b) *N* as variable.

zontal configurations are therefore shown in the following figure with thinner curves.

The effect of the inclination angle on *Nu* is presented in Fig. 9 for the case of $B = 0.3$, $C = 0.05$, $Ra = 10^6$. The upper part shows the results for $N = 2$ and various k_r, and the lower part for $k_r = 10$ and various N. The upper part shows that *Nu* increases first with increasing inclination angle from the horizontal position in which the warmer bounding wall is at the bottom. It passes from a maximum at a different angle for each k_r. The angle of the maxima is about 60 deg for $k_r = 10$, increasing first with increasing k_r, and decreasing later, which indicates a characteristic k_r for a maximum heat transfer. This observation is similar to that made earlier regarding the effect of k_r in Fig. 4. Then, *Nu* decreases with increasing angle approaching one for the horizontal case in which the warmer bounding wall is at the upper side and the heat transfer is dominated by conduction. The lower part shows that *Nu* follows the same trend as a function of Φ, as discussed above for various *N* with $k_r = 10$. The location of maximum heat transfer varies similarly with *N*, and the heat transfer becomes dominated by conduction with Φ approaching 180 deg and with increasing partition number *N*. These results are confirmed with the general observations and comments made earlier in Fig. 2.

Effect of *N*

The effect of the partition number on the heat transfer at various Rayleigh numbers is shown in Fig. 10 for the case of Φ = 60 and 0 deg, $C = 0.01$, $k_r = 5$. The results with Φ = 60 deg in the lower part of the figure shows that the heat transfer is dominated by conduction at low *Ra* numbers. This trend continues at higher *Ra* numbers with increasing *N*. Also, the heat transfer decreases with increasing *N*, as expected from earlier observations. The results with Φ = 0 deg show similar trends with increased conduction regime at higher *Ra* numbers. This is expected in view of the observations made for Fig. 2. A cross plot of *Nu* as a function of *N* with variable *C* showed that the heat transfer became dominated by conduction with increasing *N* and *C*. For a given *C* there was an upper limit of *N*, where the heat transfer became by conduction only and there was no need to add new partitions to decrease the heat transfer.

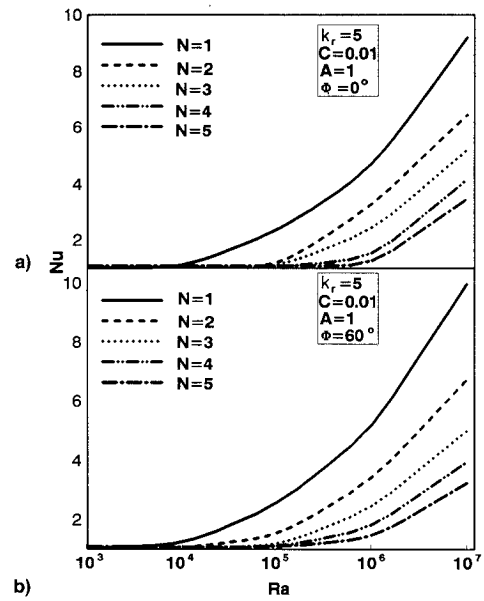

Fig. 10 Heat transfer *Nu* as a function of *Ra* with *N* as a parameter. Φ = a) 0 and b) 60 deg.

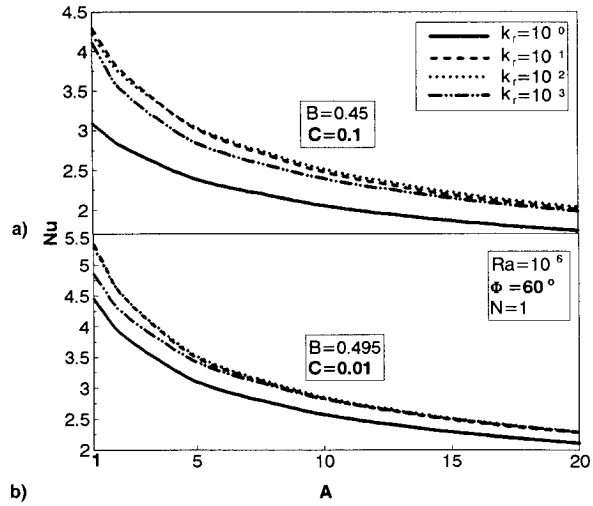

Fig. 11 Heat transfer *Nu* as a function of aspect ratio *A* for the case of $Ra = 10^6$, Φ = 60 deg, $N = 1$: a) $B = 0.460$, $C = 0.10$ and b) $B = 0.495$, $C = 0.01$.

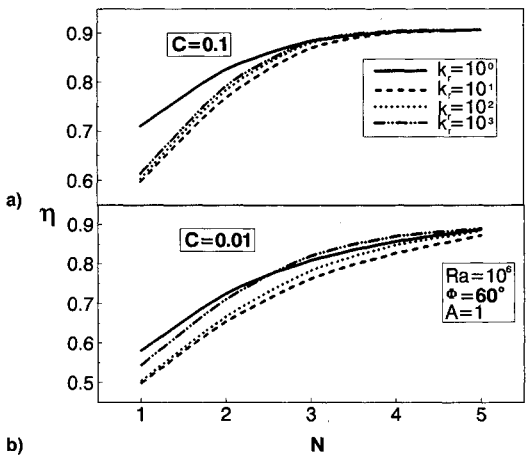

Fig. 12 Efficiency of partitions as a function of partition number N for the case of $Ra = 10^6$, $\phi = 60$ deg, $A = 1$, and various k_r. C = a) 0.10 and b) 0.01.

Effect of A

The effect of A (varied from 1 to 20) on the heat transfer is presented in Fig. 11 for the case of $Ra = 10^6$, $\Phi = 60$ deg, $N = 1$, and for various B, C, and k_r. Generally, Nu is a decreasing function of A, i.e., the natural convection is less violent in tall cavities. This is also the case with increasing C, since the aspect ratio of the individual cavities becomes bigger with increasing C. Figure 11 shows that k_r dependence of Nu is clearly observable and the critical k_r varies with A.

Efficiency of Partitions

The results of Fig. 11 and of the other similar cases can be used to calculate the efficiency of using partitions in reducing heat transfer in differentially heated cavities. The reduction in heat transfer is defined as

$$\eta = 1 - Nu_N/Nu_{N=0} \tag{11}$$

Figure 12 shows the efficiency as a function of the partition number for $k_r = 1$–1000, $C = 0.10$, 0.01, $A = 1$ at $Ra = 10^6$, and $\Phi = 60$ deg. The efficiency is generally an increasing function of N. Following earlier observations, the dependence of efficiency on k_r varies with C and N. For smaller C where the natural convection is a more dominant heat transfer mode, the efficiency of partitions becomes smaller. For example, for $C = 0.1$, the streamlines (not shown here) showed that the conduction in the partitions and in smaller cavities became increasingly more dominant heat transfer mode resulting in high efficiencies observed in Fig. 12.

Heat Transfer Correlation

The heat transfer correlation Nu as a function of the Rayleigh number Ra, aspect ratio A, conductivity ratio k_r, wall thickness C, partition number N and inclination angle Φ, was derived based on the following functional form:

$$Nu = aRa^b(1 + N)^cA^dk_r^eC^f \sin \Phi^g \tag{12}$$

where the coefficients a–g are determined by using a least-square technique as $a = 0.25$, $b = 0.25$, $c = -1$, $d = -0.25$, $e = 0.001$, $f = -0.2$, and $g = -0.1$.

The limits of the correlation are $10^5 \le Ra \le 10^7$, $0 \le N \le 5$, $1 \le A \le 5$, $1 \le k_r \le 1000$, $0.01 \le C \le 0.1$, and 30 deg $\le \varphi \le 90$ deg. The correlation coefficient R was 0.94.

It is noted that for the limiting cases of cavity without partition and with one partition, the functional form of Eq. (12) reduces to those published earlier.[7,22]

Conclusions

It is found that there is an optimum angle for a given k_r and N to maximize heat transfer in inclined cavities with multiple partitions having finite thickness and conductivity. For a given partition number, the heat transfer is dominated by conduction up to a limiting Ra number above which by convection. The heat transfer is an increasing function of k_r, up to a characteristic diffusivity above which Nu becomes a decreasing function of it. The heat transfer across the cavity can be reduced considerably by using partitions. This reduction increases with increasing partition number and thickness. However, for a given condition, there is a limiting partition number above which the reduction of heat transfer is negligible.

Acknowledgments

Financial support from the Natural Sciences and Engineering Council of Canada is acknowledged. Financial support to A. Kangni from the Canadian Fellowship Program for French Speaking Countries is also acknowledged.

References

[1]Goldstein, R. J., Chiang, H. D., and Sayer, E., "Natural Convection Mass Transfer in an Inclined Enclosure at High Rayleigh Number," *Proceedings of the 2nd International Symposium on Transport Phenomena in Turbulent Flows*, 1987, pp. 229–255.

[2]Nakamura, H., Asaka, Y., and Hirata, T., "Natural Convection and Thermal Radiation in Enclosures with a Partition Plate," *Transactions of the Japanese Society of Mechanical Engineers*, Vol. B50, 1984, pp. 2647–2654.

[3]Tong, T. W., and Gerner, F. M., "Natural Convection in Partitioned Air-Filled Rectangular Enclosures," *International Communications in Heat and Mass Transfer*, Vol. 13, 1986, pp. 99–108.

[4]Acharya, S., and Tsang, C. H., "Natural Convection in a Fully Partitioned, Inclined Enclosure," *Numerical Heat Transfer*, Vol. 8, No. 4, 1985, pp. 407–428.

[5]Anderson, R., and Bejan, A., "Heat Transfer Through Single and Double Vertical Walls in Natural Convection: Theory and Experiment," *International Journal of Heat and Mass Transfer*, Vol. 24, No. 4, 1981, pp. 1611–1620.

[6]Jones, I. P., "Numerical Predictions from the IOTA 2 Code for Natural Convection in Vertical Cavities," American Society of Mechanical Engineers Paper 82-HT-70, Dec. 1980.

[7]Nishimura, T., Shiraishi, M., Nagasawa, F., and Kawamura, Y., "Natural Convection Heat Transfer in Enclosures with Multiple Vertical Partitions," *International Journal of Heat and Mass Transfer*, Vol. 31, No. 8, 1988, pp. 1679–1686.

[8]Nishimura, T., Shiraishi, M., and Kawamura, Y., "Natural Convection Heat Transfer in Enclosures with an Off-Center Partition," *International Journal of Heat and Mass Transfer*, Vol. 30, No. 8, 1987, pp. 1756–1758.

[9]Kangni, A., Ben Yedder, R., and Bilgen, E., "Natural Convection and Conduction in Enclosures with Multiple Vertical Partitions," *International Journal of Heat and Mass Transfer*, Vol. 34, No. 11, 1991, pp. 2819–2825.

[10]Chen, W.-M., Shaw, H. J., and Huang, M. J., "Natural Convection in Partitioned Enclosed Spaces of Solar Collector," *Wärme und Stoffübertragung*, Vol. 25, No. 1, 1990, pp. 59–67.

[11]Zrikem, Z., and Bilgen, E., "Theoretical Study of a Composite Trombe-Michel Wall Solar Collector System," *Solar Energy*, Vol. 39, No. 5, 1987, pp. 409–419.

[12]Ozoe, H., Sayama, H., and Churchill, S. W., "Natural Convection in Inclined Square Channel," *International Journal of Heat and Mass Transfer*, Vol. 17, No. 3, 1974, pp. 401–406.

[13]Ozoe, H., Sayama, H., and Churchill, S. W., "Natural Convection in an Inclined Rectangular Channel at Various Aspect Ratios and Angles-Experimental Measurements," *International Journal of Heat and Mass Transfer*, Vol. 18, No. 12, 1975, pp. 1425–1431.

[14]Yang, H. Q., Yang, K. T., and Lloyd, J. R., "Laminar Natural Convection Flow Transitions in Tilted Three Dimensional Longitudinal Rectangular Enclosures," *International Journal of Heat and Mass Transfer*, Vol. 30, No. 8, 1987, pp. 1637–1644.

[15]Ozoe, H., Yamamoto, K., and Churchill, S. W., "Three Dimensional Numerical Analysis of Natural Convection in an Inclined

Channel with a Square Cross Section," *AIChE Journal*, Vol. 25, 1979, pp. 709–716.

[16]Patankar, S. V., *Numerical Heat Transfer and Fluid Flow*, Hemisphere, 1980.

[17]Ben Yedder, R., and Bilgen, E., "Natural Convection and Conduction in Trombe Wall Systems," *International Journal of Heat and Mass Transfer*, Vol. 34, Nos. 4/5, 1991, pp. 1237–1248.

[18]De Vahl Davis, G., and Jones, I. P., "Natural Convection in a Square Cavity: A Comparison Exercise," *International Journal for Numerical Methods in Fluids*, Vol. 3, No. 3, 1983, pp. 227–248.

[19]Le Breton, P., Caltagirone, J. P., and Arquis, E., "Natural Convection in a Square Cavity with Thin Porous Layers on Its Vertical Walls," *Journal of Heat Transfer*, Vol. 113, No. 4, 1991, pp. 892–898.

[20]Hasnaoui, M., Bilgen, E., and Vasseur, P., "Multiplicity of Solutions and Heat Transfer by Natural Convection in a Rectangular Cavity Partially Heated from Below," *Journal of Thermophysics and Heat Transfer*, Vol. 6, 1992, pp. 255–264.

[21]Kimura, S., and Bejan, A., "The Heatline Visualization of Convective Heat Transfer," *Journal of Heat Transfer*, Vol. 105, No. 4, 1983, pp. 916–919.

[22]Bejan, A., *Convection Heat Transfer*, Wiley, New York, 1984.